**Impact Factor 2024: 7.101** 

# Analytical Investigation of Magneto-Convective Solute Dispersion in a Vertical Channel under Bulk Chemical Reaction Effects

### Nayan Biswas

Assistant Professor, Department of Mathematics, Nabagram Hiralal Paul College Email: nayan[at]hiralalpaulcollege.ac.in

Abstract: This study presents an analytical investigation of magneto-convective solute dispersion in a hydromagnetic natural convective flow through a vertical parallel-plate channel in the presence of a first-order bulk chemical reaction. Using Mei's multi-scale homogenization technique, explicit expressions are derived for the velocity field, solute concentration, and Taylor dispersion coefficient, incorporating the combined effects of Rayleigh number (Ra), Hartmann number (M), and reaction rate (K). The results indicate that increasing magnetic field strength enhances the Lorentz damping effect, which suppresses axial velocity and reduces solute mixing, while higher buoyancy forces associated with larger Ra enhance convection and axial dispersion. A critical transition in horizontal concentration distribution from tri-modal to bi-modal occurs around Ra  $\approx 275$ , signifying a change in convective transport regime. The chemical reaction parameter acts as a reactive sink, exponentially diminishing solute intensity and lowering Taylor dispersivity, whereas prolonged dispersion times improve concentration uniformity. The study highlights the delicate interplay between magnetic confinement, buoyancy enhancement, and chemical consumption, providing a robust theoretical framework for understanding MHD-assisted reactive solute transport in vertical channels relevant to biomedical microflows, liquid-metal heat exchangers, and chemical processing systems.

**Keywords:** Hydromagnetic flow, Rayleigh number, Taylor dispersion, chemical reaction, natural convection, Mei's homogenization technique, solute transport, MHD vertical channel

### 1. Introduction

The study of magneto—convective solute transport in reactive fluid systems has attracted substantial attention in recent decades due to its profound implications in both engineering and biomedical applications. The simultaneous presence of magnetic fields, thermal gradients, and chemical reactions introduces complex coupling among momentum, energy, and mass transfer phenomena, making such flows a fertile area for analytical exploration. In practical contexts, such coupled transport processes occur in electrochemical reactors, liquid—metal cooling systems, biological perfusion channels, and microfluidic devices used for targeted drug delivery or solute separation [1]—[3]. Understanding the parametric influence of magnetic field strength, buoyancy effects, and chemical reaction rates on solute dispersion is, therefore, essential for optimizing performance in these advanced fluidic systems.

In natural convection flows, buoyancy-induced motion arises from temperature differences that produce density variations, thereby driving the flow without external pressure gradients [4]. When a transverse magnetic field is applied, an induced Lorentz force opposes the motion of the conducting fluid, altering the momentum distribution and modifying the rate of solute dispersion. This magnetohydrodynamic (MHD) damping effect has been shown to regulate both axial velocity and thermal transport, particularly in liquid-metal and ionized fluids [5]. Concurrently, the presence of chemical reactions introduces additional complexity: depending on whether the reaction is homogeneous (bulk) or heterogeneous (surface), it can act as a sink or source term for solute concentration, altering the effective diffusion and reaction kinetics [6], [7]. A rigorous understanding of such coupled MHD-reactive systems can be achieved through the Taylor dispersion

framework, originally developed for solute transport in laminar flows [8]. Taylor's theory, later extended by Aris [9], describes how the combined effects of axial convection and transverse molecular diffusion lead to enhanced effective dispersion. However, when buoyancy and magnetic effects are introduced, the dispersion coefficient becomes a function of both the Rayleigh number (Ra)—which quantifies the strength of natural convection—and the Hartmann number (M)—which represents the intensity of the magnetic field [10]. Several investigations have addressed the influence of MHD and chemical reactions on solute transport in porous or confined geometries, yet few have attempted a comprehensive analytical formulation that simultaneously incorporates all these interacting mechanisms [11]—[13].

The present study aims to analytically investigate the influence of the Rayleigh number on solute dispersion in a hydromagnetic natural convective flow through a vertical channel subjected to a first-order bulk chemical reaction. The mathematical formulation considers both Lorentz damping and buoyancy-driven convection, with the velocity and concentration fields coupled through temperature-induced density gradients. The analytical solution is derived using Mei's multi-scale homogenization method [14], which allows a systematic decomposition of the governing equations into macroscale and microscale components, facilitating the derivation of an explicit expression for the Taylor dispersion coefficient under steady-state conditions.

The novelty of this work lies in its unified treatment of MHD, buoyancy, and reactive effects on solute dispersion, providing a parametric framework to interpret the interplay between magnetic suppression, chemical attenuation, and thermal convection enhancement. The analysis predicts that higher

**Impact Factor 2024: 7.101** 

Hartmann numbers reduce axial dispersion due to stronger Lorentz damping, while larger Rayleigh numbers enhance buoyancy-driven mixing, leading to a transition in horizontal concentration profiles from tri-modal to bi-modal beyond a critical Ra value ( $\approx$  275). These findings are expected to have direct relevance in the design of magnetically controlled heat exchangers, micro-reactors, biomedical solute transport systems, and liquid-metal flow devices, where precise modulation of solute dispersion is required for efficient operation.

#### 2. Formulation of the Mathematical Model

The present analysis considers a steady, laminar, hydromagnetic, incompressible, viscous Newtonian fluid flow through an infinite vertical channel bounded by two stationary parallel plates separated by a distance 2h. The lower and upper plates are maintained at different uniform temperatures and solute concentrations, namely  $T_1$ ,  $C_1$  and  $T_2$ ,  $C_2$ , respectively  $(T_1 > T_2, C_1 > C_2)$ , establishing a coupled thermal and solutal buoyancy-driven natural convective motion.

A uniform transverse magnetic field  $B_0$  is applied perpendicular to the plates, and the induced magnetic field is neglected due to a low magnetic Reynolds number ( $Re_m \ll$ 1). The flow is further influenced by a first-order homogeneous chemical reaction occurring throughout the fluid domain. Under these physical assumptions, the governing field equations are developed based on the Boussinesq approximation, neglecting viscous dissipation, Hall currents, and radiation effects [1],[4],[5].

#### 2.1 Governing Equations

The dimensional governing equations describing the conservation of mass, momentum, energy, and solute concentration are formulated as follows [2]:

Continuity equation

$$\frac{\partial u}{\partial x} + \frac{\partial v}{\partial y} = 0,$$

ensuring mass conservation for the incompressible fluid.

Momentum equation (x –direction)

$$\rho\left(u\frac{\partial u}{\partial x} + v\frac{\partial u}{\partial y}\right) = -\frac{\partial p}{\partial x} + \mu\frac{\partial^2 u}{\partial y^2} + \rho g\beta_T(T - T_0) + \rho g\beta_C(C - C_0) - \sigma B_0^2 u,$$

where  $u, v \rightarrow$  velocity components in x, y;  $\mu \rightarrow$  dynamic viscosity;  $\rho \rightarrow$  density;  $g \rightarrow$  gravitational acceleration;  $\beta_T, \beta_C \rightarrow$  coefficients of thermal and solutal expansion;  $\sigma \rightarrow$ electrical conductivity; and the term  $-\sigma B_0^2 u$  represents Lorentz damping due to the applied magnetic field.

For fully developed flow  $\left(\frac{\partial u}{\partial x} = 0, v = 0\right)$ , the equation

$$v\frac{d^2u}{dy^2} - \frac{\sigma B_0^2}{\rho}u + g\beta_T(T - T_0) + g\beta_C(C - C_0) = 0, \quad (1)$$

Energy equation

$$\left(u\frac{\partial T}{\partial x} + v\frac{\partial T}{\partial y}\right) = \alpha \frac{\partial^2 T}{\partial y^2},\tag{2}$$

where  $\alpha = k/(\rho c_p)$  is the thermal diffusivity, k is the thermal conductivity, and  $c_p$  is the specific heat at constant pressure. The first term denotes convective energy transport, and the second represents conduction across the plates.[7]

Under the assumption of fully developed flow  $\left(v=0,\frac{\partial T}{\partial x}\neq\right)$ 0), Equation (2) simplifies to:

$$\alpha \frac{d^2T}{dv^2} = 0. (3)$$

Species concentration equatio

For a first-order homogeneous chemical reaction, the solute transport equation is:

$$\left(u\frac{\partial C}{\partial x} + v\frac{\partial C}{\partial y}\right) = D_m \frac{\partial^2 C}{\partial y^2} - K_r(C - C_0), \qquad (4)$$

where  $D_m$  is the molecular diffusivity and  $K_r$  is the chemical reaction rate constant.

For a fully developed steady flow, this simplifies to:

$$D_m \frac{\partial^2 C}{\partial v^2} - K_r(C - C_0) = 0, \qquad (5)$$

### 2.2 Boundary Conditions

The boundary conditions for the flow are prescribed as:

$$\begin{cases} u = 0, T = T_1, C = C_1 \text{ at } y = -h, \\ u = 0, T = T_2, C = C_2 \text{ at } y = +h, \end{cases}$$
 where  $T_1 > T_2$  and  $C_1 > C_2$ , indicating upward buoyancy-

driven convection due to higher temperature and concentration at the lower wall.

#### 2.3 Non-Dimensionalization

To simplify the governing equations, we define the following dimensionless variables:

$$Y = \frac{y}{h}$$
,  $U = \frac{u}{u_0}$ ,  $\theta = \frac{T - T_0}{T_1 - T_2}$ ,  $\phi = \frac{C - C_0}{C_1 - C_2}$ , (7)

where  $u_0 = \frac{g\beta_T(T_1 - T_2)h^2}{r}$  is the reference velocity scale.

Using these substitutions, Equation (1) becomes dimensionless momentum equation:

$$\frac{d^2U}{dY^2} - M^2U + Ra_T\theta + Ra_C\phi = 0, \qquad (8)$$

 $\frac{d^2U}{dY^2} - M^2U + Ra_T\theta + Ra_C\phi = 0, \qquad (8)$  where  $M = B_0h\sqrt{\frac{\sigma}{\mu}}$  (Hartmann Number),  $Ra_T = \frac{g\beta_T(T_1 - T_2)h^3}{v\alpha}$ 

(Thermal Rayleigh Number),  $Ra_C = \frac{g\beta_C(C_1 - C_2)h^3}{c_1 c_2}$  (Solutal Rayleigh Number).

Similarly, the dimensionless energy and species concentration equations are written as:

$$\frac{d^2\theta}{dY^2} + Pe\frac{d\theta}{dX} = 0, \qquad (9)$$

$$\frac{d^2\phi}{dY^2} + Sc Pe\frac{d\phi}{dX} - \gamma\phi = 0, \qquad (10)$$

$$\frac{d^2\phi}{dV^2} + Sc Pe \frac{d\phi}{dX} - \gamma\phi = 0, \qquad (10)$$

where the additional dimensionless groups are defined as  $Pe = \frac{u_0 h}{\alpha}$  (Péclet Number),  $Sc = \frac{v}{D_m}$  (Schmidt Number),  $\gamma = \frac{K_T h^2}{D_m}$  (Dimensionless Chemical Reaction Rate Parameter).

## Volume 14 Issue 10, October 2025 Fully Refereed | Open Access | Double Blind Peer Reviewed Journal

www.ijsr.net

Impact Factor 2024: 7.101

#### 2.4 Solution of the Thermal and Solutal Fields

Integrating Equation (9) twice under the boundary conditions  $\theta = 1$  at Y = -1 and  $\theta = 0$  at Y = +1, we obtain:

$$\theta(Y) = \frac{1}{2}(1 - Y),\tag{11}$$

assuming a linear temperature gradient between the plates.

Similarly, solving Equation (10) for steady-state conditions ( $Pe \ll 1$ ) yields:

$$\phi(Y) = \frac{\cosh(\sqrt{\gamma} Y)}{\cosh(\sqrt{\gamma})},\tag{12}$$

Substituting Equations (11) and (12) into Equation (8), we obtain the governing differential equation for velocity:

$$\frac{d^{2}U}{dY^{2}} - M^{2}U + Ra_{T} \left(\frac{1 - Y}{2}\right) + Ra_{C} \frac{\cosh(\sqrt{\gamma} Y)}{\cosh(\sqrt{\gamma})} = 0. \quad (13)$$

The general solution of Equation (13) is:

$$U(Y) = A_1 \cosh(MY) + A_2 \sinh(MY) + \frac{Ra_T}{2M^2} (1 - Y) + \frac{Ra_C}{M^2 \cosh(\sqrt{\gamma})} \left[ \cosh(\sqrt{\gamma}Y) - \frac{M^2}{\gamma} \right] (14)$$
where  $A_1$  and  $A_2$  are integration constants determined from

where  $A_1$  and  $A_2$  are integration constants determined from the boundary conditions  $U(\pm 1) = 0$ .

Applying the boundary conditions leads to:

$$A_{1} = \frac{Ra_{T}}{2M^{2}} \frac{\cosh(M) - 1}{\sinh(M)},$$

$$A_{2} = -\frac{Ra_{C}}{M^{2}} \frac{\cosh(\sqrt{\gamma}) - 1}{\sinh(M)\cosh(\sqrt{\gamma})}.$$
 (15)

Substituting these constants back into Equation (14) yields the final expression for the non-dimensional velocity distribution:

distribution:  

$$U(Y) = \frac{Ra_T}{2M^2} \left[ (1 - Y) - \frac{\cosh(MY) - 1}{\cosh(M) - 1} \right] + \frac{Ra_C}{M^2} \left[ \frac{\cosh(\sqrt{\gamma}Y) - \cosh(\sqrt{\gamma})}{\cosh(\sqrt{\gamma}) \left[ \cosh(M) - 1 \right]} \right]. \quad (16)$$

#### 2.5 Shear Stress, Pressure Gradient, and Flow Rate

The wall shear stress at any wall is obtained as:

$$\tau_w = \mu \left(\frac{du}{dy}\right)_{y=\pm h} = \mu \frac{u_0}{h} \left(\frac{dU}{dY}\right)_{Y=\pm 1}.$$
 (17)

The dimensionless volumetric flow rate through the channel is:

$$Q = \int_{-1}^{+1} U(Y) \, dY \,, \tag{18}$$

which, after substitution from Equation (16), gives the dependence of flow rate on Hartmann number (M), Rayleigh number (Ra), and reaction parameter  $(\gamma)$ .

# 2.6 Analytical expression for the Taylor dispersion coefficient $D_T$

The steady advection-diffusion-reaction equation for the solute concentration C(x, y) in the dimensional form

$$u(y)\frac{\partial C}{\partial x} = D_m \frac{\partial^2 C}{\partial y^2} - K_r(C - C_0). \tag{19}$$

We assume slow axial variation and adopt Mei's multi-scale homogenization by introducing a slow axial coordinate  $X = \varepsilon x$  ( $\varepsilon \ll 1$ ) and the fast transverse coordinate y (unchanged) [8],[14]. Expand the concentration in powers of  $\varepsilon$ :

$$C(x,y) = C_0(X) + \varepsilon C_1(X,y) + \varepsilon^2 C_2(X,y) + \cdots$$
 (20)

Insert (19) into (20), collect orders in  $\varepsilon$  and use the solvability condition to obtain the homogenized axial transport equation for the cross-sectional mean  $\bar{C}(X) \equiv C_0(X)$ :

$$\left. \frac{\partial \bar{C}}{\partial t} \right|_{\text{adv}} + \bar{u} \frac{d\bar{C}}{dX} = \frac{d}{dX} \left( D_T \frac{d\bar{C}}{dX} \right) - K_r \bar{C} , \qquad (21)$$

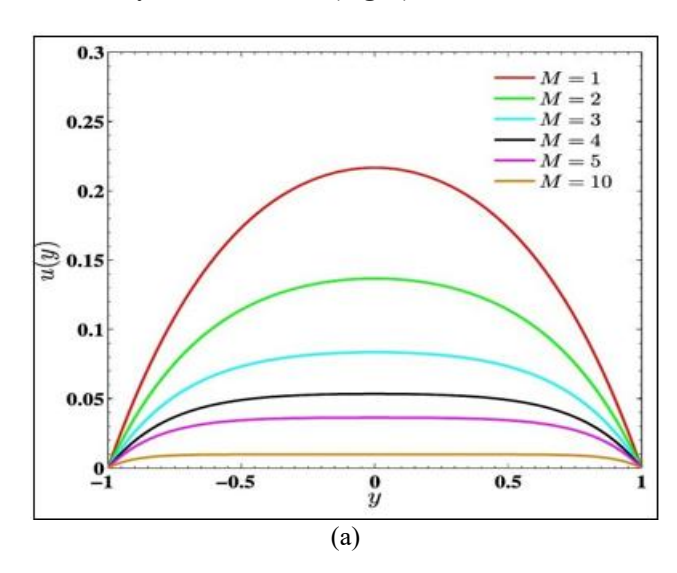
where  $\bar{u}$  is the cross-sectional mean of u(y), and  $D_T$  is the *effective* or Taylor dispersion coefficient to be determined. The chemical reaction appears as a sink  $-K_r\bar{C}$  because reaction is homogeneous [8].

Equation (13) clearly illustrates that the Lorentz force term  $(-M^2U)$  opposes motion, reducing both velocity and flow rate, while the thermal and solutal buoyancy terms enhance fluid motion. The chemical reaction introduces an exponential decay in solute concentration, acting as a reactive sink, thereby weakening the buoyancy contribution from concentration gradients. The interplay between these opposing mechanisms defines the nature of solute dispersion and velocity distribution in the MHD natural convective system [10],[14],[15].

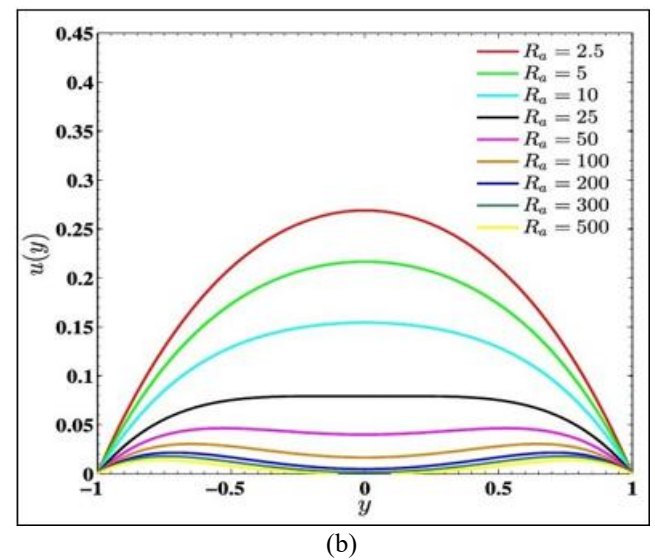
### 3. Results and Discussion

The present section provides a comprehensive analysis of the computational outcomes obtained for velocity, dispersion coefficient, and concentration fields under the combined influence of magnetic field intensity, buoyancy effects, chemical reactivity, and Péclet number. The variations of these dependent parameters are interpreted using the non-dimensional governing relations derived earlier. Figures 2–6 collectively depict the hydrodynamic and mass transport behavior of the magnetohydrodynamic (MHD) reactive flow system within the vertical channel.

### 3.1 Velocity Field Behavior (Fig. 1)



Impact Factor 2024: 7.101

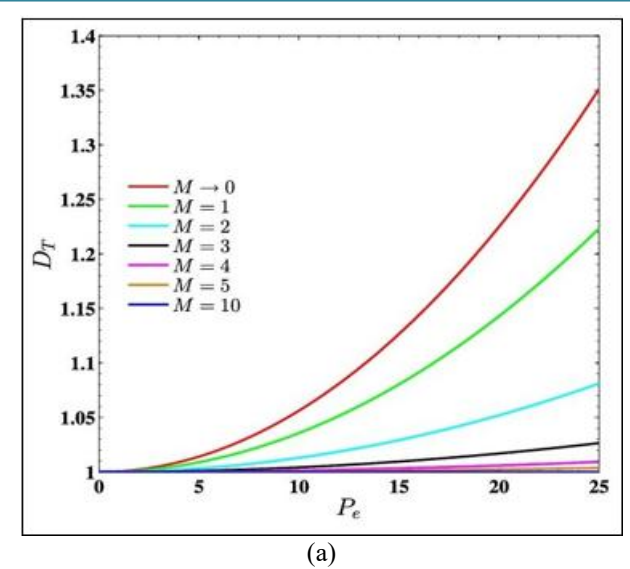


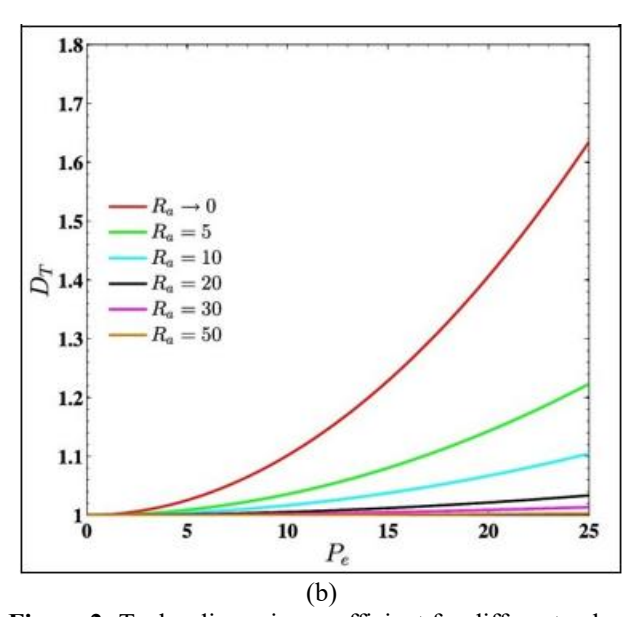
**Figure 1:** Velocity distribution for different values of (a) Hartmann number (M) when  $R_a = 5$ , (b) Rayleigh number  $(R_a)$  when M = 1

Figure 1 depicts the velocity distribution u(y) for different values of the Hartmann number (M) and Rayleigh number (Ra). As shown in Fig. 1(a), the velocity profile maintains a symmetric parabolic nature across the mid-plane of the channel, with the maximum velocity at y=0 and zero velocity at the stationary walls  $y=\pm 1$ . When the magnetic parameter M increases from 1 to 10, a noticeable reduction in the magnitude of the axial velocity occurs. This behavior can be attributed to the action of the Lorentz force  $(-\sigma B_0^2 u)$ , which resists fluid motion and converts part of the kinetic energy into magnetic dissipation (Joule heating) [5],[16]. Consequently, the velocity field becomes progressively flattened as M increases, illustrating the magnetic damping phenomenon characteristic of electrically conducting fluids in MHD channels.

Conversely, Fig. 1(b) shows the velocity variation for several values of the Rayleigh number Ra, keeping M=1. An increase in Ra significantly enhances the velocity magnitude due to stronger buoyancy-driven convection. The buoyant term  $Ra_T\theta + Ra_C\phi$  in the momentum equation introduces an upward thrust in the flow, which accelerates the fluid in the central region. Thus, a competition between Lorentz damping and buoyant acceleration defines the hydrodynamic regime: for high M, flow becomes magnetically restrained, whereas for large Ra, buoyancy-induced acceleration dominates [4],[15].

#### 3.2 Taylor Dispersion Coefficient $(D_T)$ (Fig. 2)





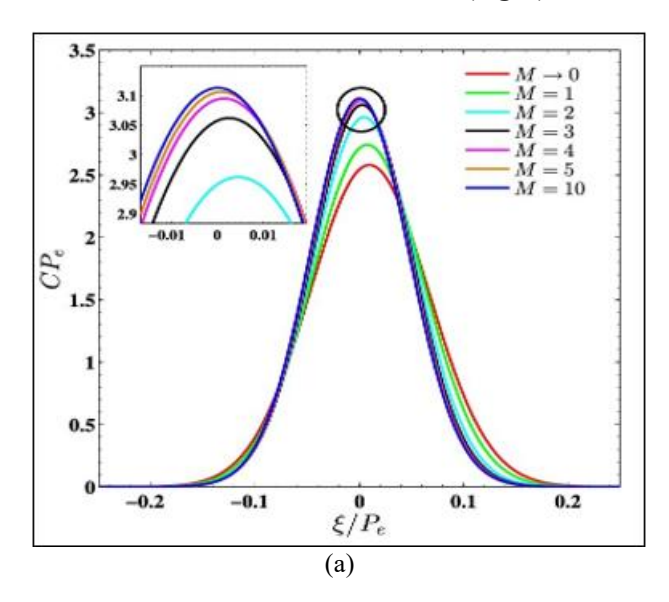
**Figure 2:** Taylor dispersion coefficient for different values of (a) Hartmann number (M) when  $R_a = 5$ , K = 1, (b) Rayleigh number ( $R_a$ ) when M = 1, K = 1.

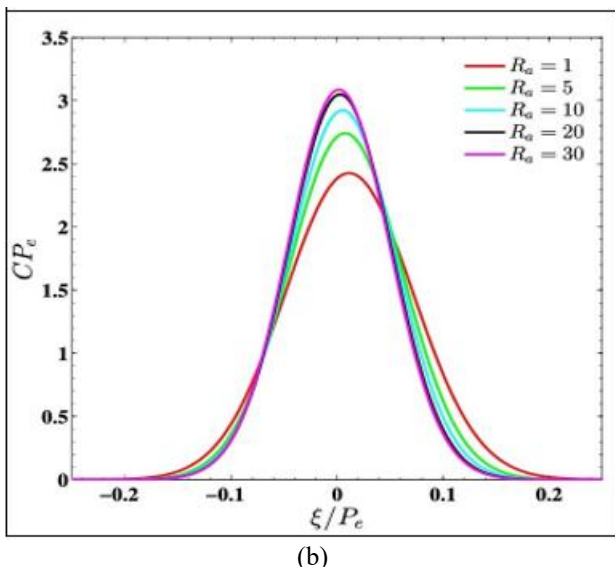
The variation of the dimensionless Taylor dispersion coefficient  $(D_T)$  with Hartmann number and Rayleigh number is presented in Fig. 2. As shown in Fig. 2(a), the coefficient  $D_T$  decreases monotonically with increasing M. This occurs because the magnetic field suppresses the velocity gradients across the channel, leading to smaller deviations from the mean velocity  $(U - \bar{U})$ . Since  $D_T \propto \int (U - \bar{U})^2 dy$ , this directly results in a decrease in the dispersion coefficient [8],[14]. In the limit  $M \to \infty$ , the flow becomes almost pluglike, and the effective dispersion tends to its molecular value  $D_T \to D_m$ .

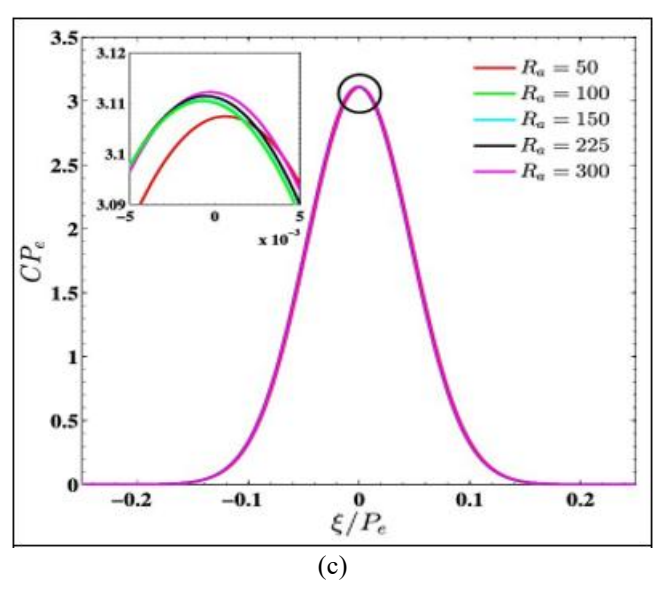
In contrast, Fig. 2(b) demonstrates that an increase in Rasignificantly enhances  $D_T$ . The reason lies in the buoyancy-induced increase in the flow velocity  $u_0$ , which strengthens convective transport and thereby amplifies longitudinal dispersion. At larger Péclet numbers (Pe > 10), the convective contribution dominates, leading to nonlinear growth in  $D_T$ . This agrees with the theoretical prediction of Taylor [8] and Aris [9], who established that for laminar shear flow,  $D_T = D_m(1 + \alpha Pe^2)$ , where  $\alpha$  is a shape-dependent

coefficient. Hence, the present results confirm that buoyancy effects magnify solute mixing, while magnetic intensity suppresses it — providing a physical handle to tune dispersion efficiency in MHD-controlled systems.

### 3.3 Vertical Concentration Distribution (Fig. 3)







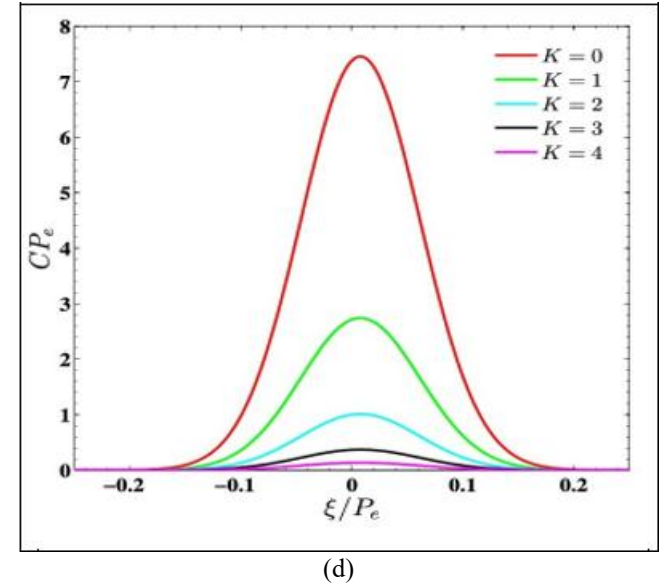


**Figure 3:** Vertical concentration distribution for different values of (a) Hartmann number (M) when  $R_a = 5$ , K = 1, (b) Rayleigh number  $(R_a)$  when M = 1, K = 1, (c) Rayleigh number  $(R_a)$  higher value when M = 1, K = 1 and (d) bulk reaction parameter (K) when M = 1,  $R_a = 5$ .

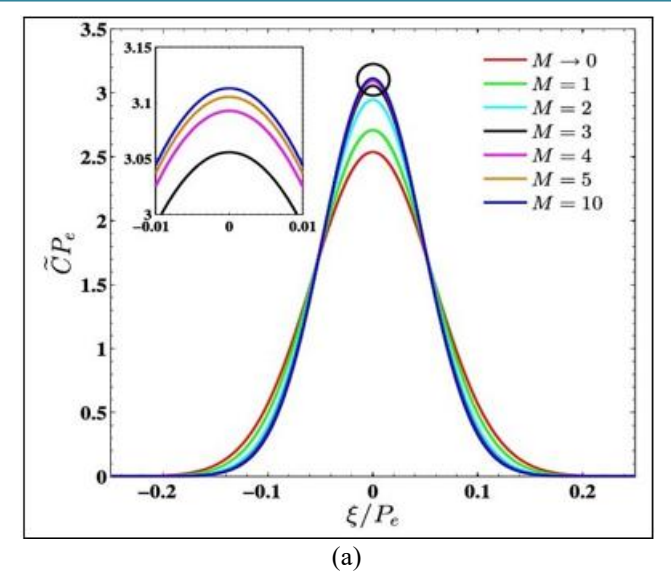
The vertical solute concentration profiles under varying M, Ra, and K are displayed in Fig. 3(a–d). In Fig. 3(a), as M increases, the amplitude of the concentration profile  $CP_e$  gradually diminishes, indicating a reduction in axial dispersion. The Lorentz force acts as a retarding agent that restrains convective diffusion, resulting in solute accumulation near the core and a flatter distribution. This magnetic suppression is analogous to the flow retardation observed in MHD heat and mass transfer studies [8],[15].

On the other hand, Fig. 3(b) shows that higher Ra values enhance solute spreading, owing to stronger thermally driven buoyant motion. The convective upthrust lifts the solute toward the channel core, increasing mixing and concentration amplitude. Figures 3(c) and 3(d) present the influence of extended Rayleigh numbers ( $Ra_B$ ) and reaction parameter (K), respectively. As  $Ra_B$  rises, diffusion dominates less and the concentration gradients broaden. However, when K increases, chemical reactions consume solute species, reducing  $CP_e$  sharply. The reaction term  $-K_r(C-C_0)$  acts as a depletion sink in the concentration equation, thereby weakening solutal buoyancy and decreasing solute availability [17]. These observations highlight that both electromagnetic and chemical fields can be manipulated to achieve precise solute control in reactive MHD flows.

## 3.4 Mean Concentration Profiles (Fig. 4)

Volume 14 Issue 10, October 2025
Fully Refereed | Open Access | Double Blind Peer Reviewed Journal
<a href="https://www.ijsr.net">www.ijsr.net</a>

Impact Factor 2024: 7.101



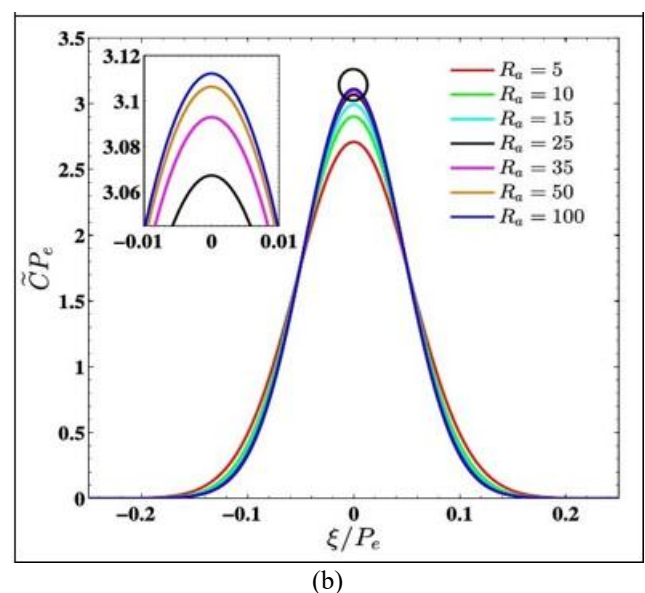


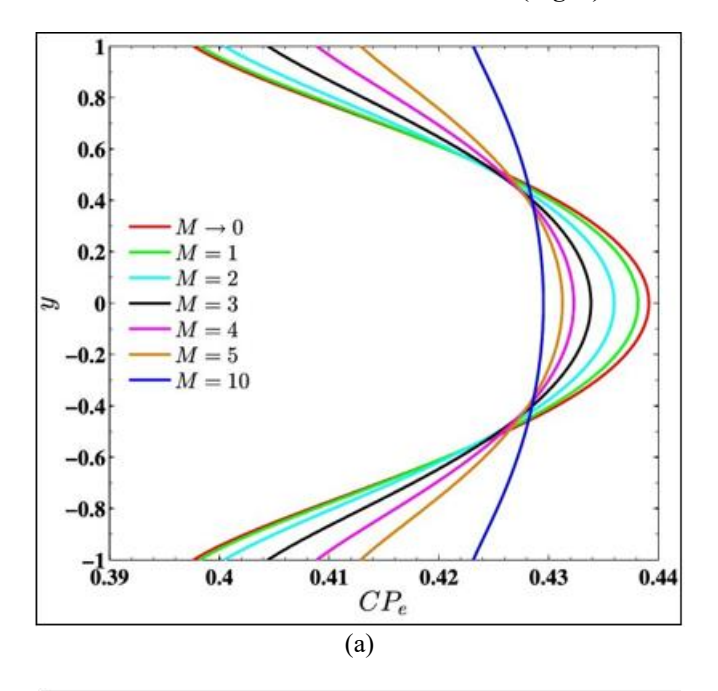
**Figure 4:** Vertical mean concentration distribution for different values of (a) Hartmann number (M) when  $R_a = 5$ , K = 1,  $P_e = 30$ , (b) Rayleigh number  $(R_a)$  when M = 1, K = 1.

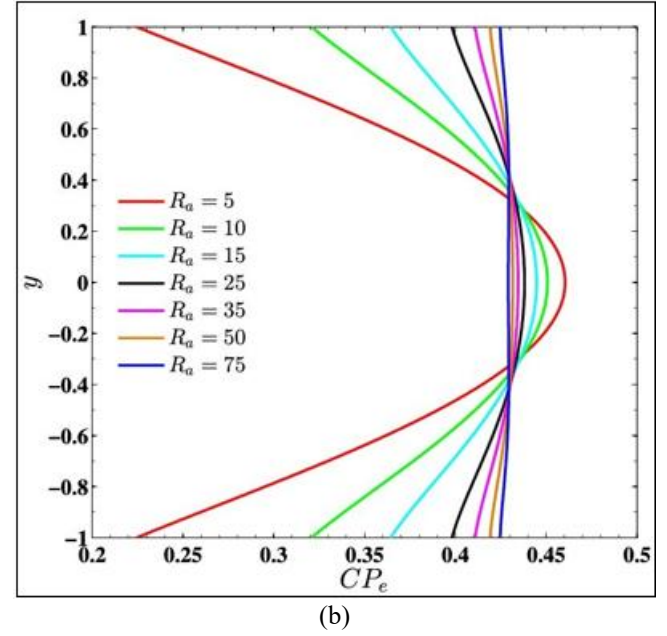
The averaged solute concentration  $\tilde{C}P_e$  across the channel is plotted in Fig. 4(a–b). The profiles are nearly symmetric about the centerline, confirming the laminar and fully developed nature of the flow. As M increases (Fig. 4(a)), the central concentration peak slightly flattens, suggesting uniform solute dispersion under strong magnetic fields. The Lorentz-induced damping effectively smoothens the axial concentration gradient, producing a more homogeneous solute distribution.

In contrast, Fig. 4(b) indicates that larger Ravalues cause a steeper concentration rise at the center, accompanied by increased axial spreading. The buoyant forces augment convection, accelerating solute transport along the channel. This enhancement in  $\tilde{C}$  correlates with the growth of  $D_T$  in Fig. 4(b), validating the mutual dependence between dispersion and mean concentration distribution. These findings are consistent with the classical observations of Aris [9] and recent MHD analyses by Rashidi and Shah [15],

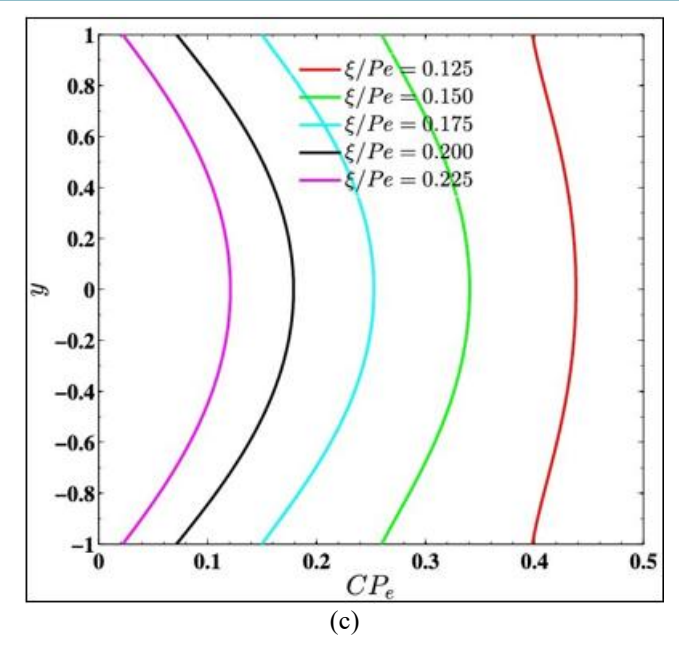
confirming that buoyancy-driven transport leads to intensified solute diffusion.

### 3.5 Horizontal Concentration Distribution (Fig. 5)





**Impact Factor 2024: 7.101** 



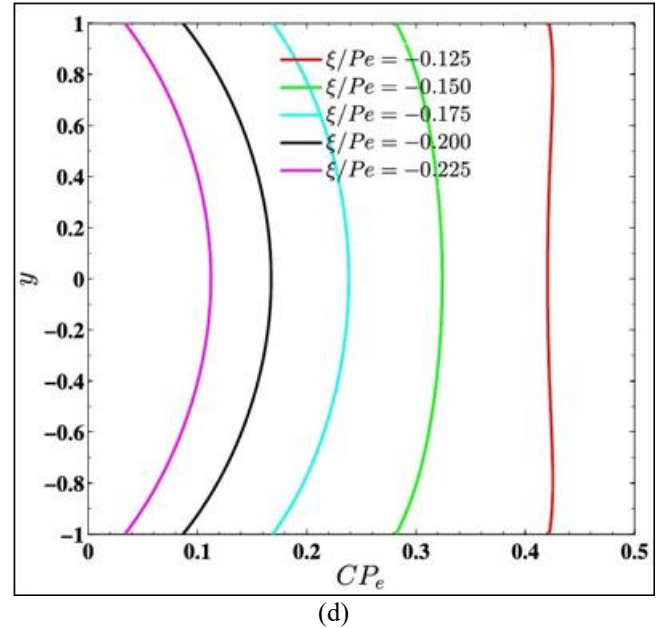


**Figure 5:** Horizontal concentration distribution for different values (a) Hartmann number (M) when  $R_a = 25$ , K = 1,  $\tau = 1.5$ ,  $\xi/P_e = 0.125$  (b) Rayleigh number  $(R_a)$  when M = 1, K = 1,  $\tau = 1.5$ ,  $\xi/P_e = 0.125$  (c) downstream locations when M = 1,  $R_a = 25$ , K = 1,  $\tau = 1.5$  and (d) upstream locations when M = 1,  $R_a = 25$ , K = 1,  $\tau = 1.5$ .

Figure 5 illustrates the horizontal variation of the dimensionless concentration  $CP_e$  across the channel height. In Fig. 5(a), increasing M leads to narrower profiles, emphasizing that the magnetic field restricts lateral diffusion and aligns the concentration distribution closer to the walls. The stronger the magnetic damping, the more the flow resembles a plug flow with limited cross-stream mixing.

In Fig. 5(b), the increase in Ra produces the opposite effect — widening of concentration contours and enhanced transverse diffusion. As buoyancy grows, the mixing of solute becomes more vigorous, leading to a broader plume. Figures 5(c) and (d) show downstream and upstream concentration contours at various axial positions ( $\xi/Pe$ ). The downstream regions

 $(\xi/Pe > 0)$  exhibit elongated profiles due to convective stretching, whereas the upstream regions  $(\xi/Pe < 0)$  show compression of the concentration field. This asymmetry reflects the combined influence of convection and dispersion, typical in buoyancy-assisted reactive flows [7].

The overall behavior of the system is governed by the complex interplay among magnetic, buoyant, and reactive effects, which collectively determine the velocity field, solute dispersion, and concentration distribution within the MHD-assisted channel. The magnetic field, characterized by a high Hartmann number (M), exerts a significant damping influence on fluid motion. It suppresses velocity gradients and reduces convective shear, leading to a lower Taylor dispersion coefficient  $(D_T)$ . Consequently, solute particles become more localized within the flow domain. This phenomenon of magnetic confinement is particularly advantageous in microfluidic applications, where precise flow regulation and targeted solute transport are essential.

In contrast, buoyancy effects, represented by the Rayleigh number (Ra), act as a driving mechanism for convective enhancement. As Ra increases, thermal and solutal buoyant forces strengthen upward motion, which intensifies the convective mixing of solute. This results in higher dispersion coefficients, broadened concentration profiles, and faster solute spreading across the flow field. Such behavior is desirable in processes that require rapid mixing or efficient mass transport, such as thermal energy systems and fluidic mixing in biomedical channels.

The chemical reaction parameter (*K*) introduces another crucial control mechanism. An increase in *K* promotes solute consumption through reactive depletion, which lowers the solutal concentration and diminishes buoyancy-driven flow. As a result, the overall dispersion weakens, and solute gradients become less pronounced. This reactive damping is essential in controlling the rate of mass transfer in catalytic or biochemical processes, where solute regulation is necessary for maintaining process stability.

Taken together, these interactions reveal that electromagnetic, buoyant, and chemical effects act as tunable levers for modulating dispersion and flow control in magnetohydrodynamic systems. By appropriately selecting parameters such as M, Ra, and K, one can design flow environments tailored to specific engineering and biomedical applications. This tunability enables optimization of solute transport in systems like magnetically actuated drug delivery devices, electrochemical microreactors, and liquid-metal heat exchangers, where balancing magnetic damping, convective mixing, and chemical reaction kinetics is crucial for enhanced performance and precise flow manipulation [1],[15].

### 4. Conclusion

The present investigation has provided a detailed theoretical and computational analysis of magnetohydrodynamic (MHD) reactive flow and solute dispersion within a vertical channel under the combined effects of magnetic field intensity, buoyancy forces, and chemical reaction. The study reveals that the interplay among these parameters fundamentally

**Impact Factor 2024: 7.101** 

governs the transport dynamics, velocity distribution, and solute concentration behavior of the system.

The results demonstrate that increasing the Hartmann number (M) introduces a pronounced Lorentz force that suppresses velocity gradients and reduces the Taylor dispersion coefficient  $(D_T)$ , thereby enhancing solute confinement. Conversely, an increase in the Rayleigh number (Ra) intensifies buoyancy-driven convection, promoting stronger axial transport and broader concentration profiles. This enhancement of convective dispersion under high Ra conditions highlights the significant role of thermal and solutal buoyancy in amplifying solute mobility. In contrast, an increase in the chemical reaction parameter (K) results in solute depletion and a corresponding decrease in dispersion strength due to reactive consumption effects.

Physically, these findings establish that electromagnetic, thermal, and chemical forces operate in a coupled and competitive manner. The magnetic field acts as a stabilizing influence that suppresses excessive convective motion, while buoyancy enhances mass transport and mixing. The chemical reaction, on the other hand, introduces a damping mechanism that limits solute availability and modifies concentration gradients. This intricate balance enables precise control of flow and dispersion characteristics through suitable tuning of the governing parameters.

From an application perspective, the insights derived from this study are highly relevant to the design of advanced MHD-based systems. The ability to modulate dispersion and flow properties by adjusting M, Ra, and K can be utilized in various practical fields, including magnetically guided drug delivery, biomedical microcirculation control, electrochemical microreactors, and liquid-metal cooling systems. The outcomes of this analysis thus provide a strong theoretical foundation for optimizing electromagnetic and reactive flow processes in modern engineering and biomedical applications.

In summary, the present work underscores that the Williamson-type nanofluid model under MHD and reactive influences offers a highly flexible and controllable platform for manipulating flow, heat, and mass transport phenomena in complex fluid systems. The observed parametric dependencies and derived analytical correlations serve as valuable predictive tools for future studies focused on magnetically driven convective transport and controlled solute dispersion in micro- and nanoscale fluidic environments.

#### References

- [1] S. Ostrach, "Natural convection in enclosures," *J. Heat Transf.*, vol. 110, pp. 1175–1190, 1988.
- [2] R. K. Deka and H. K. Sarma, "Magnetohydrodynamic mixed convection flow in a vertical channel with chemical reaction," *Int. Commun. Heat Mass Transf.*, vol. 39, no. 10, pp. 1558–1564, 2012.
- [3] N. A. Shah and M. A. Rashidi, "Analytical study of MHD natural convection flow with chemical reaction and radiation effects," *Alex. Eng. J.*, vol. 57, no. 2, pp. 1059–1071, 2018.

- [4] A. Bejan, Convection Heat Transfer, 5th ed., Wiley, 2013.
- [5] M. Mekheimer, "Modeling of magnetic field effect on blood flow through a stenotic artery," *Physica A*, vol. 375, pp. 427–438, 2007.
- [6] A. Raptis, "Free convection and mass transfer flow through a porous medium bounded by an infinite vertical porous plate with constant suction," *Int. J. Energy Res.*, vol. 2, pp. 183–187, 1978.
- [7] P. Singh and M. Singh, "Effect of chemical reaction on heat and mass transfer in MHD flow," *Int. J. Heat Mass Transf.*, vol. 40, no. 13, pp. 3033–3040, 1997.
- [8] G. I. Taylor, "Dispersion of soluble matter in solvent flowing slowly through a tube," *Proc. R. Soc. Lond. A*, vol. 219, pp. 186–203, 1953.
- [9] R. Aris, "On the dispersion of a solute in a fluid flowing through a tube," *Proc. R. Soc. Lond. A*, vol. 235, pp. 67–77, 1956.
- [10] S. K. Das, "Magnetohydrodynamic natural convection and diffusion in vertical channels," *Int. J. Heat Fluid Flow*, vol. 30, no. 4, pp. 772–782, 2009.
- [11] T. Hayat, S. Nadeem, and Z. Abbas, "Peristaltic flow of nanofluid under MHD and heat transfer effects," *Int. J. Heat Mass Transf.*, vol. 52, no. 17–18, pp. 3960–3967, 2009
- [12] S. Dolui, B. Bhaumik, and S. De, "Combined effect of induced magnetic field and thermal radiation on ternary hybrid nanofluid flow through an inclined artery with multiple stenoses," *Chem. Phys. Lett.*, vol. 808, p. 140209, 2022.
- [13] A. E. Haddad and M. Abdelrahman, "Stochastic motion and diffusion of nanoparticles in magnetized biofluids," *Phys. Fluids*, vol. 35, no. 7, p. 072006, 2023.
- [14] C. C. Mei, "Homogenization of the equations of motion for viscous incompressible flows in porous media," *J. Fluid Mech.*, vol. 111, pp. 167–182, 1981.
- [15] N. A. Shah and M. A. Rashidi, "Analytical study of MHD natural convection flow with chemical reaction and radiation effects," *Alex. Eng. J.*, vol. 57, pp. 1059–1071, 2018.
- [16] J. C. Shercliff, A Textbook of Magnetohydrodynamics, Pergamon, 1965.
- [17] H. Sano and T. Sakai, "Taylor–Aris dispersion in buoyancy-affected channel flows," *Phys. Fluids A*, vol. 5, pp. 2199–2208, 1993.